Combustion and Flame 212 (2020) 135–141

Contents lists available at ScienceDirect

Combustion and Flame

journal homepage: www.elsevier.com/locate/combustflame

The kinetic study of excited singlet oxygen atom O(^{1}D) reactions with acetylene

Chao Yan[a,*], Chu C. Teng[b], Timothy Chen[a], Hongtao Zhong[a], Aric Rousso[a], Hao Zhao[a], Guoming Ma[a,c], Gerard Wysocki[b], Yiguang Ju[a]

[a] Department of Mechanical and Aerospace Engineering, Princeton University, Princeton, NJ, 08544, USA
[b] Department of Electrical Engineering, Princeton University, Princeton, NJ, 08544, USA
[c] State Key Laboratory of Alternate Electrical Power System with Renewable Energy Sources, North China Electric Power University, Beijing 102206, China

ARTICLE INFO

Article history:
Received 29 March 2019
Revised 30 April 2019
Accepted 25 October 2019
Available online 9 November 2019

Keywords:
Singlet oxygen atom
Photolysis Herriott cell
Faraday rotation spectroscopy
Balanced detection
Plasma assisted combustion

ABSTRACT

Understanding the multi-channel dynamics of O(^{1}D) reactions with unsaturated hydrocarbon molecules in low temperature reaction kinetics is critically important in stratospheric chemistry, plasma chemistry, plasma assisted fuel reforming, materials synthesis, and plasma assisted combustion. A photolysis flow reactor coupled with highly selective mid-infrared Faraday Rotation Spectroscopy (FRS) and direct ultraviolet-infrared (UV-IR) absorption spectroscopy (DAS) techniques was developed for the first time to study the multi-channel dynamics of excited singlet oxygen atom O(^{1}D) reactions with C_2H_2 and the kinetics of subsequent reactions. Time-resolved species concentrations of OH, HO_2 and H_2O were obtained and used to develop a validated kinetic model of O(^{1}D) reactions with C_2H_2. The branching ratios of O(^{1}D) reaction with C_2H_2 and subsequent HO_2 kinetics were also quantified. It is found that, contrary to O(^{1}D) reactions with saturated alkanes, OH formation via direct H abstraction by O(^{1}D) is negligible. The results revealed that two chain-branching and propagation reactions via direct O(^{1}D) insertion are the major pathways for radical production. The present study clearly demonstrated the advantage of radical detection and kinetic studies using FRS in the effective suppression of absorption interference from non-paramagnetic hydrocarbons.

1. Introduction

The chemical behavior of electronically excited singlet oxygen atom, O(^{1}D), is of considerable interest and remains experimentally attractive throughout the past few decades due to its substantial roles in establishing chemical composition of atmospheric chemistry, plasma fuel reforming, plasma assisted materials synthesis and plasma assisted combustion [1–5]. Numerous studies [3–5] have shown that O(^{1}D) atoms contribute significantly to enhance ignition, reform fuel, and reduce emissions. In particular, O(^{1}D) plays an important role in accelerating low temperature chain branching, leading to the formation of cool flames and warm flames [4,6]. Moreover, O(^{1}D) also contributes to the oxidation of leaked fuels and unburned hydrocarbons as well as the O_3 cycle in the atmosphere [7,8]. As such, understanding the multi-channel dynamics of the O(^{1}D) reaction with fuel molecules and the low temperature reaction kinetics is critical. However, O(^{1}D) reactions with fuels are complicated by its multi-channel behavior due to direct oxygen atom insertion process.

Early studies [9–14] of the reaction between O(^{1}D) with saturated hydrocarbons have been conducted to understand the role of O(^{1}D) initiated chain-branching reactions. In reaction dynamic studies, the products and branching ratios of the reaction channels are quite different because of the competition among different channels after oxygen atom insertion. In these reactions, the dominant reaction mechanism is the oxygen atom insertion into C-H bond, while direct H abstraction in the OH formation channel and oxygen atom insertion into the C-C bond are also important in some cases for larger hydrocarbons.

Unfortunately, for even a simple unsaturated hydrocarbon such as C_2H_2, the multi-channel dynamics of its reaction with O(^{1}D) and the kinetics of subsequent reactions are not well understood. Limited relevant studies [15–17] were performed to determine the overall rate constant and estimate the chain-branching products. The determined rate constant is $k(O(^1D) + C_2H_2) = (3.1 \pm 0.2) \times 10^{-10}$ cm^3 molecule^{-1} s^{-1}. Based on this estimation [16], four potential reaction channels are considered in the current reaction mechanism:

* Corresponding author.
E-mail address: chaoy@princeton.edu (C. Yan).

https://doi.org/10.1016/j.combustflame.2019.10.034
0010-2180/

$$O(^1D) + C_2H_2 \longrightarrow HCCOH \quad R1a \tag{1}$$

$$O(^1D) + C_2H_2 \longrightarrow HCCO + H \quad R1b \tag{2}$$

$$O(^1D) + C_2H_2 \longrightarrow CH_2(S) + CO \quad R1c \tag{3}$$

$$O(^1D) + C_2H_2 \longrightarrow C_2H + OH \quad R1d \tag{4}$$

In addition, the radicals formed during these secondary chain-branching reactions initialize further chain-propagation and chain-branching reactions. Formation of radicals (e.g. OH and HO_2) due to the subsequent hydrocarbon oxidation reactions are therefore extremely important. Understanding the multi-channel dynamics and subsequent reaction kinetics of $O(^1D)$ with C_2H_2 is critical to understanding $O(^1D)$ kinetics with larger unsaturated fuels and unburned hydrocarbons typically containing alkenes and aldehydes.

Time-resolved diagnostics of radical species is crucial in kinetic studies due to the short-lived nature of free radicals. Many spectroscopic techniques have been adopted for radical species detection, the most notable examples include ultraviolet (UV) and mid-infrared (IR) tunable laser absorption spectroscopy (TDLAS), laser-induced fluorescent spectroscopy (LIF), and cavity ring-down spectroscopy (CRDS) [18–24]. For LIF, HO_2 is measured indirectly through chemical conversion to OH, and in many cases uncontrolled reactions involving the peroxy radicals introduce significant experimental uncertainty. Moreover, the sensitivity and uncertainty are limited by fluorescence quenching when the gas pressure is high. Therefore, calibrations are required at each pressure points [21,22].

For CRDS, the acquisition interval is limited by the time required to have sufficient intensity build-up in the cavity and radical quenching on the sampling nozzle [23]. TDLAS in principle can provide much better time resolution; however, sensitive measurement of radicals (e.g. RO_2 and HO_2) in both CRDS and TDLAS is challenging due to spectral contaminations from H_2O_2, H_2O, and other hydrocarbons in the mid-IR and UV regions [25,26]. Typically, the efficacy of TDLAS depends on identifying a spectral region free from unwanted absorption features, which becomes challenging in higher pressure experiments, and is compounded when using larger fuels with broadband spectral features [18,23,27].

To this end, Brumfield et al. first applied Faraday rotation spectroscopy (FRS) for HO_2 detection at the exit of a laminar flow reactor [27]. A modulated magnetic field was used to improve the detection limit and remove spectral interference. However, no time dependent measurements were attempted due to the slow field modulation.

In this work, we aim to study the multi-channel dynamics of excited singlet oxygen atom $O(^1D)$ reactions with C_2H_2 and the kinetics of subsequent reactions via selective and time resolved detection of HO_2 and OH radicals by using FRS in a balanced detection scheme [28] to effectively cancel common-mode spectral interference.

2. Methodology

In this study, we developed a new photolysis flow reactor to study the reactions between $O(^1D)$ and C_2H_2 by combining mid-infrared FRS with direct UV-IR TDLAS (Fig. 1).

The reactor is made of quartz tubing with an inner diameter of 56 mm. A pair of spherical mirrors with 250 mm focal length are installed at the both ends of the reactor 913 mm apart to form the multi-pass configuration (MPC), also called Herriot configuration for the QCLs (7.2 µm, Thorlabs and 2.8 µm, Nanoplus) beams. The mirror substrate is UV-grade CaF_2, offering $>$ 90 % transmission from UV to 7.1 µm. A protective gold coating extends 8 mm from the edge of the mirror, leaving a 20° section transparent for the IR probe beam to couple into the photolysis cell. The uncoated central part of the spherical mirrors, 40 mm in diameter, allows for the UV photolysis beam to pass through the cell. Two dichroic mirrors (OMEGA OPTICAL) mounted at 45° are placed at the entrance and exit of the flow reactor to allow coupling of both UV photolysis beam and O_3 monitor beam (HG-1 Ocean Optics) in a single-pass configuration. A beam expander consisting of a UV coated plano-concave lens (f = −30 mm) and a UV coated plano-convex lens (f = 200 mm) were used to improve the homogeneity of the photolysis beam. The resulting photolysis beam profile was measured using an energy meter (NOVA II) combined with a diaphragm (ca. 1 mm) over the entire area of the beam. An iris diaphragm was installed at the entrance of the reactor with 18 mm diameter. Generally, the center part of the laser beam has better uniformity, therefore the iris diaphragm cut the laser beam and only allowed relatively uniform laser light passing through the reactor. The measured UV beam profile indicates that the uniformity across the reactor cross-section is ± 8.4 % from the mean value.

Currently the MPC is set up in a 21-pass configuration, resulting in an effective pathlength of 6.3 m after taking into consideration the overlap between the 25 mm diameter photolysis beam and the IR probe beam. The time resolved absorption signals of OH radicals and HO_2 radicals are measured using DFB-QCLs centered around the spectral regions of 3568.52 cm^{-1} and 1396.91 cm^{-1}, respectively. For HO_2 detection using FRS, the laser frequency is scanned over the absorption features of interest via current modulation at 10 kHz, and the concentration of HO_2 is obtained from spectral fitting with a time resolution of 100 µs. For OH detection, we identified an interference free region around 3568.52 cm^{-1}, as a result better temporal resolution (up to 1 µs) can be obtained by operating the laser in continuous mode at fixed laser current.

A kinetic model is developed based on HP-Mech [29,30] with electronically excited species sub-mechanism. The updated HP-Mech was attached in the supplementary material, in which the $O(^1D)$ and electronically excited oxygen molecule $O_2(^1\Sigma)$ quenching reactions and reactions with O_3, H_2, H_2O_2, CH_4, H_2O, CH_2O, H, H_2O, CH_3 and C_2H_2 were considered. The half-life of diffusion time for major radicals and atoms out of photolysis beam (50 ms-100 ms) are more than five times larger than HO_2 radicals decay time (ca. 10 ms) and almost two orders longer compared with OH radical decay time (ca. 1 ms). Thus, the photolysis reactor could be simulated by using closed homogeneous batch reactor (0-D) in Chemkin.

The absolute concentrations of $O(^1D)$ and the absolute concentration of radicals are critical in order to determine the branching ratios of reaction $O(^1D)$ with C_2H_2. The absolute concentration of $O(^1D)$ was varied ca. 2 times and quantified by measuring the photon flux inside the reactor [1,26] using the absorption cross-section and the photolysis reaction pathway of O_3 at 266 nm at 60 Torr and 296 K. Ozone concentration is measured by a photomultiplier tube (Hamamatsu R7154) with amplifier (Hamamatsu C6271) using DAS signals from the monochromator (Acton 2500i). To avoid interferences from residual photolysis light or fluorescence from any surface, a 254 nm mercury line filter (Semrock) is installed before the monochromator. The major source of uncertainty in determining absolute concentration of $O(^1D)$ is quantifying the photolysis laser intensity inside the reactor. Therefore, we used *in-situ* laser light actinometry based on ozone depletion, which is relatively stable at these conditions, with detailed characterization of the cross-section at the monitoring wavelength of 253.65 nm (Mercury line) [31]. Ozone depletion in this measurement occurs in two stages, as seen in Fig. 2. The first stage is direct photolysis depletion: $O_3 + h\nu \longrightarrow O(^1D) + O_2$ and $O_3 + h\nu \longrightarrow O(^3P) + O_2$. The second stage is chemical reaction consumption: a decay in ozone concentration due to excited oxygen atoms $O(^1D)$ and excited

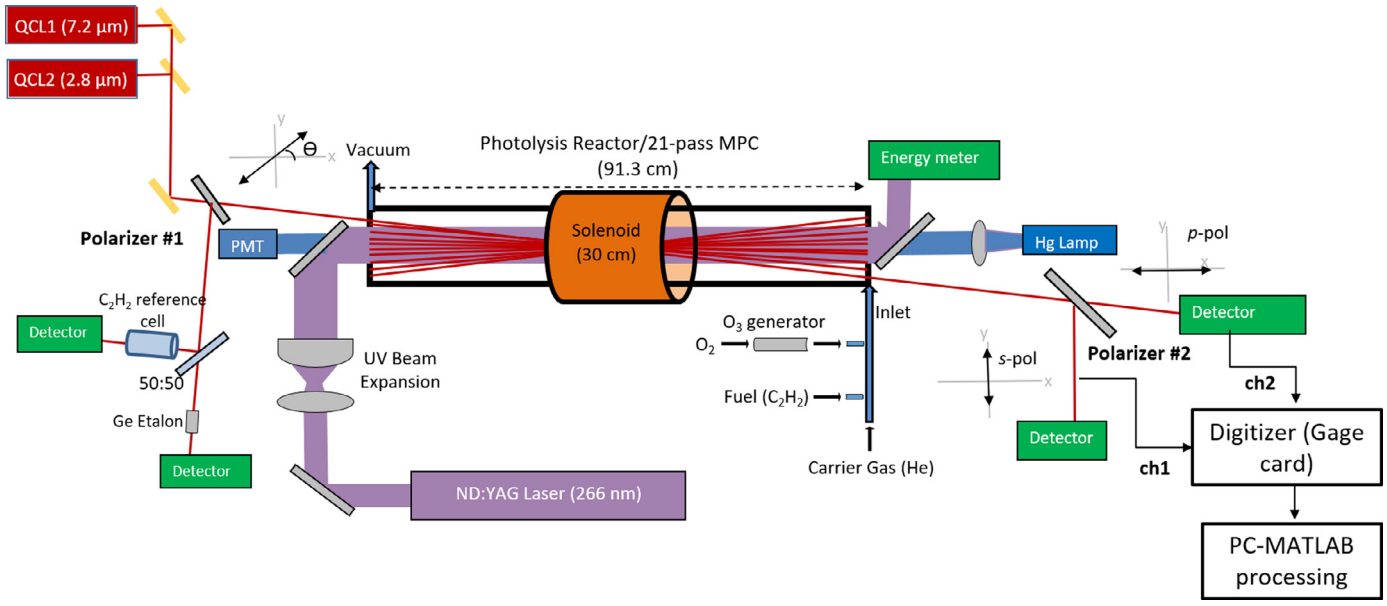

Fig. 1. Experimental setup schematic.

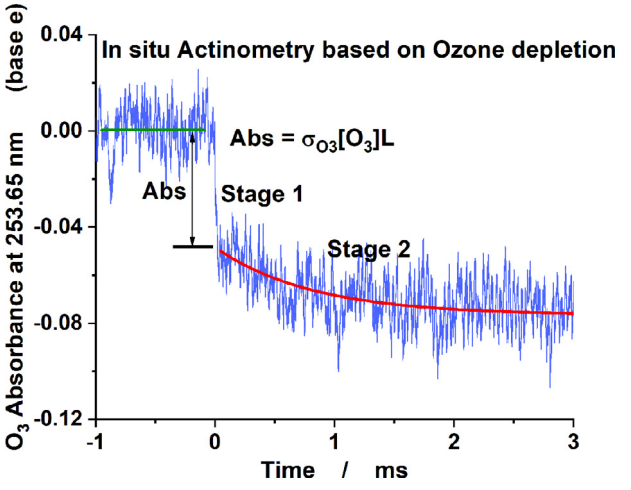

Fig. 2. *In-situ* actinometry based on ozone depletion. Ozone is detected at the monitoring wavelength of 253.65 nm (Mercury line). Ozone depletion in this measurement occurs in two stages. The first stage is direct photolysis depletion; the second stage is secondary chemical reaction consumption. Green line is linear fitting before UV photolysis. Red line is fitted by HP-Mech which photon fluence is fitting parameter.

oxygen molecules $O_2(^1\Sigma)$ interaction with O_3. The main reactions for stage 2 are: $O(^1D) + O_2 \longrightarrow O(^3P) + O_2(^1\Sigma)$, $O_2(^1\Sigma) + O_3 \longrightarrow O(^3P) + 2O_2$ and $O(^1D) + O_3 \longrightarrow 2O_2$. The photon fluence F (photons cm^{-2}) can be calculated based on the absorbance (Abs):

$$F = \frac{Abs}{\sigma_{O_3,253.65} * L * [O_3] * \sigma_{O_3,266}} \quad (5)$$

where the ozone absorption cross-sections at 253.65 nm and 266 nm are:

$$\sigma_{O_3,253.65} = (1.136 \pm 0.012) \times 10^{-17} cm^2 molecule^{-1} \quad (6)$$

$$\sigma_{O_3,266} = (9.04 \pm 0.64) \times 10^{-18} cm^2 molecule^{-1} \quad (7)$$

L = 913 mm is the length of the reactor, and $[O_3]$ is the concentration. Actinometry measurements were performed before spectroscopy experiments to provide the absolute concentration of $O(^1D)$ atoms.

In the presence of a paramagnetic species such as HO_2, magnetically induced circular birefringence (MCB) causes rotation of the polarization plane of linearly polarized light, which leads to the FRS signal. As Fig. 1 shows, a solenoid is used to generate an axial magnetic field (370 Gauss) along the direction of laser propagation within the flow reactor. A pair of wire-grid polarizers are used: one defines the incident linear polarization, and the second serves as an analyzer to convert laser polarization rotation into intensity changes that can be detected using photodetectors. In this case, the analyzer (Polarizer #2) axis is rotated at an angle of 45° with respect to the initial polarizer (Polarizer #1), hence the exit beam is split into the s and p orthogonal polarizations in the transmitted and reflected beam. In this balanced detection configuration, the FRS signal is obtained from the differential measurement between the s and p polarizations while other signals, including non-paramagnetic absorptions, appear as common mode signal [32,33].

The advantage of this detection scheme is demonstrated in Fig. 3, where we compare the TDLAS absorption spectra and FRS spectra observed at 7.2. μm under the same experimental conditions. Figure 3(a) shows the saw-tooth laser frequency scanning across the HO_2 transitions at a rate of 10 kHz, leading to an acquisition time of 100 μs for each spectrum. A total of 5 consecutive spectra are shown here, with ozone photolysis initiated after the second ramp. The TDLAS spectra is shown in panel (b), where 4 C_2H_2 lines are clearly visible and labeled in the figure. After the photolysis reactions, the HO_2 absorption signal appears near a dominant C_2H_2 transition as also labeled in panel (b). At 60 Torr, the HO_2 signal is still distinguishable from C_2H_2 but is already affected by the C_2H_2 lines. This spectral interference is effectively suppressed in the FRS signal as shown in panel (c), where HO_2 formation is clearly visible after photolysis starts. HO_2 concentration is determined by least mean square fitting to the FRS spectrum using HITRAN line parameters. Due to the use of helium as the bath gas, collisional line-broadening parameters deviate from the air-broadening coefficients provided by HITRAN. Based on a well-calibrated frequency axis using a Germanium etalon, the actual broadening coefficient is determined during the nonlinear fitting procedure based on the best fit to the measured spectrum.

It should be noted that at higher pressures, collisional line broadening will result in more severe overlap between this interference and the HO_2 absorption signal, therefore the immunity

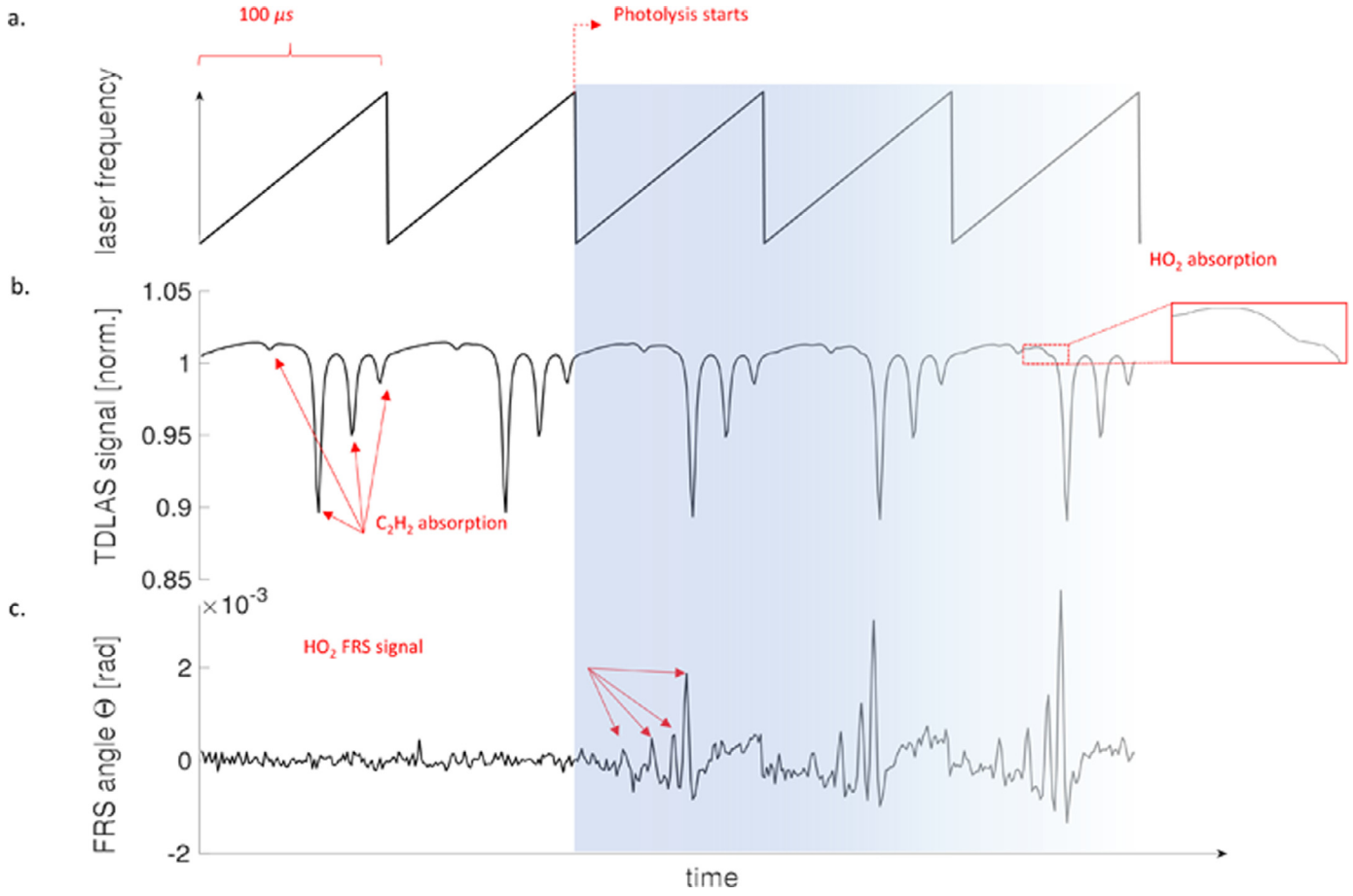

Fig. 3. Illustration of spectral interference removal using FRS. (a) Continuous linear laser frequency scanning at a rate of 10 kHz from 1396.8 cm^{-1} to 1396.95 cm^{-1}. A total of 5 consecutive spectra are recorded with UV photolysis initiated after the second ramp. (b) TDLAS spectra containing both C_2H_2 and HO_2 absorption signal with prominent C_2H_2 features in the same spectral region. A zoomed view of HO_2 absorption is shown to emphasize the magnitude of spectral interference compared to the HO_2 signal using TDLAS. c) FRS spectra measured in the same experimental condition as (b). Note the absence of non-paramagnetic C_2H_2 absorptions.

to spectral interference from non-paramagnetic species makes FRS a uniquely suitable technique for *in-situ* measurements of radical species over a wide range of experimental conditions (e.g. with varying pressure and different fuels). In addition, given the clean signal spectrum achievable using FRS, spectral line-fitting is not required to isolate the HO_2 signal, which would be critical in the case shown in panel (b). Hence line-locked harmonic detection can be performed using fast laser wavelength modulation (e.g. at 100 kHz) to further improve sensitivity and time resolution of FRS detection [34].

In addition to HO_2, time-resolved concentration measurements of OH and H_2O are also required for modeling the chemical reaction pathways. In the current setup, another QCL at 2.8 μm is used for measuring OH and H_2O generated during the reactions following ozone photolysis. Since negligible spectral interference between OH and nearby water lines is observed at the current pressure conditions (60 Torr 150 Torr), TDLAS is used for detecting both OH and H_2O. QCL laser frequency fluctuations up to 0.003 nm is observed during the OH measurements. Since this fluctuation is 4 times smaller than the full width at half maximum (FWHM) of OH absorption profiles at 60 Torr and 296 K according to HITRAN simulations, insignificant influence to concentration retrieval is assumed. The absorption cross-section of the OH radical at 3568.52 cm^{-1} is calibrated using well studied chemical reactions $O_3 + h\nu \longrightarrow O(^1D) + O_2$ and $O(^1D) + H_2O \longrightarrow 2OH$ (Fig. 4). The obtained absorption cross section is:

$$\sigma_{OH,3568.52\,cm-1} = (3.1 \pm 0.5) \times 10^{-18} cm^2 molecule^{-1} \quad (8)$$

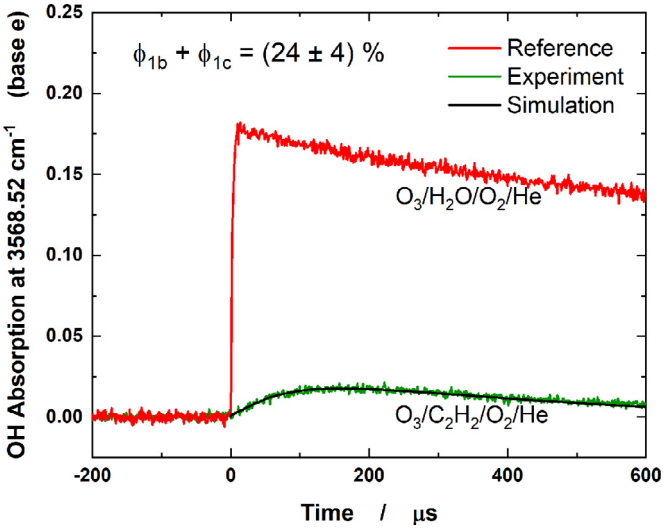

Fig. 4. Comparison of the 60 Torr experimental data and simulation based on updated HP-Mech. $[C_2H_2] = 1.69 \times 10^{16}$ molecules cm^{-3}. $[O_2] = 6.32 \times 10^{15}$ molecules cm^{-3}. $[O_3] = 2.94 \times 10^{14}$ molecules cm^{-3}. $[H_2O] = 9.23 \times 10^{16}$ molecules cm^{-3}. $[O(^1D)] = 5.88 \times 10^{13}$ molecules cm^{-3}. The time-resolved measurements of OH radicals. The absorption cross-section of the OH radical at 3568.52 cm^{-1} is calibrated using well studied chemical reactions $O_3 + h\nu \longrightarrow O(^1D) + O_2$ and $O(^1D) + H_2O \longrightarrow 2OH$ (Reference). In this experimental condition, the recombination channel is dominant (branching ratio $\phi 1a = 76$ %), while channel $O(^1D) + C_2H_2 \longrightarrow C_2H + OH$ (R1d) can be neglected.

It should be noted, however, that with minor modifications to the current system, OH detection using FRS can be implemented to allow measurements at higher reactor pressures where interference becomes significant. The absorption cross section of H_2O at 3568.29 cm^{-1} is:

$$\sigma_{H_2O}, 3568.29\text{cm} - 1 = 2.45 \times 10^{-19}\text{cm}^2\text{molecule}^{-1} \quad (9)$$

at 60 Torr, which is taken from the HITRAN database [35].

All the experiments were carried out at 60 Torr and 150 Torr pressure and ambient temperature. The gas flow rates were controlled by mass flow controllers (MKS instruments). Helium was used as the bath gas to dilute the reactant mixtures with total flow rate in the range of 2300 sccm – 12300 sccm. Liquid H_2O (10 – 30 µl / min) was injected through a precision syringe pump (Harvard Apparatus, Model PHD 2200), which was delivered through a capillary tube into a heated pre-vaporization chamber maintained at 90 °C. O_3 was produced by an ozone generator (Ozone Solutions, TG-20) from the downstream of O_2 flow. The Nd:YAG laser (Quantel Laser, Qsmart 850) was operated at 0.2 – 1 Hz repetition rate. The Q-switch output signal was used as trigger signal for oscilloscope to acquire data.

The concentration of O_3 in the gas mixture in the range of (1.2 – 3.3) × 10^{14} molecules cm^{-3}, allowing only a small fraction of the photolysis beam (less than 30%) to be absorbed to maintain homogeneous photolysis light throughout the reactor. The concentration of C_2H_2 in the range of (1.2 – 2.5) × 10^{16} molecules cm^{-3}, which was in excess compared to that of $O(^1D)$ ((3.8 - 7.5) × 10^{13} molecules cm^{-3}). O_2 concentration was in the range of (2.4 - 6.5) × 10^{15} molecules cm^{-3}. The photon fluence inside the reactor was in the range of (2.1 – 3.7) × 10^{16} photons cm^{-2}.

Reagents: All gases used in this study were obtained from Airgas. Ultra High Purity (UHP) helium 99.9995 % purity was used as the bath gas in all the experiments. Atomic Absorption (AA) grade acetylene 99.6% purity was well mixed with the bath gas before entering the reactor. UHP oxygen 99.994% purity was the precursor for ozone generation. Deionized water was injected through precision syringe pump after freeze-pump-thaw procedure degassed.

3. Results and discussion

Transient absorption profiles of OH and HO_2 were measured at 60 Torr pressure and ambient temperature, which are shown in Figs. 4–6. To determine the branching ratios of reaction ($O(^1D) + C_2H_2$), a reaction mechanism based on the HP-mech was used to model and simulate the experimental profiles. The transient absorption profiles were simulated by numerical solutions of a system of differential equations corresponding to the reaction mechanism using Chemkin-Pro software [36].

The reaction rate constants used in the reaction mechanism and absorption cross sections were taken from literature and measured in the current work. The updated HP-Mech reaction mechanism used in the model are listed in the supporting documents. The formation of OH radicals is dominated by the reaction of H + O_3 and most H atoms react with O_3 molecules. The H atoms are contributed by the initial dissociation of the HCCOH and two major secondary reactions (HCCO+O_2 and $CH_2 + O_2$) in which HCCO radicals are the major products of dissociation of HCCOH (reaction R1b) and majority $CH_2(S)$ formed in reaction R1c are quenched by He and C_2H_2 to form CH_2 in less than 1 µs time scale. The total contribution of all other reactions in terms of formation of OH is less than 6% at 60 Torr and ambient temperature. The decay of OH radicals is almost entirely controlled by the two reactions (the major channel: C_2H_2+OH and the minor channel: $HO_2 + OH$). The rest of the reactions in the mechanism (updated HP-Mech) only places minor roles and can make some small corrections.

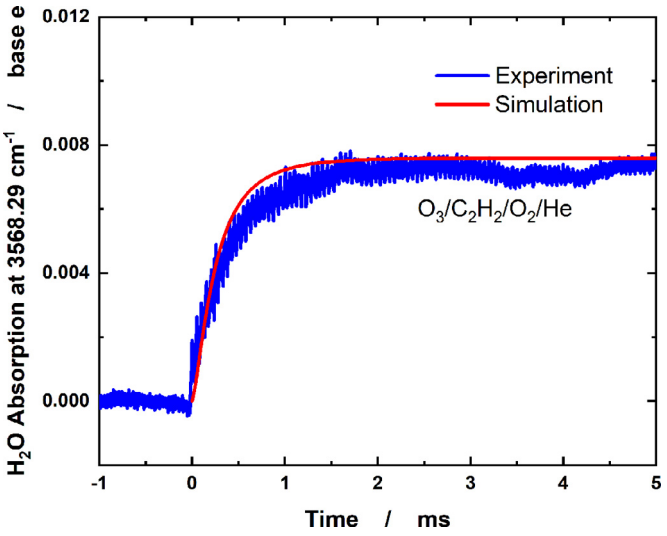

Fig. 5. The time-resolved measurement of H_2O was measured at 3568.29 cm^{-1} wavenumber. There is good agreement between the experimental measurement and theoretical simulation based on the updated HP-Mech. [C_2H_2] = 1.42 × 10^{16} molecules cm^{-3}. [O_2] = 6.27 × 10^{15} molecules cm^{-3}. [O_3] = 1.26 × 10^{14} molecules cm^{-3}. [$O(^1D)$] = 4.50 × 10^{13} molecules cm^{-3}.

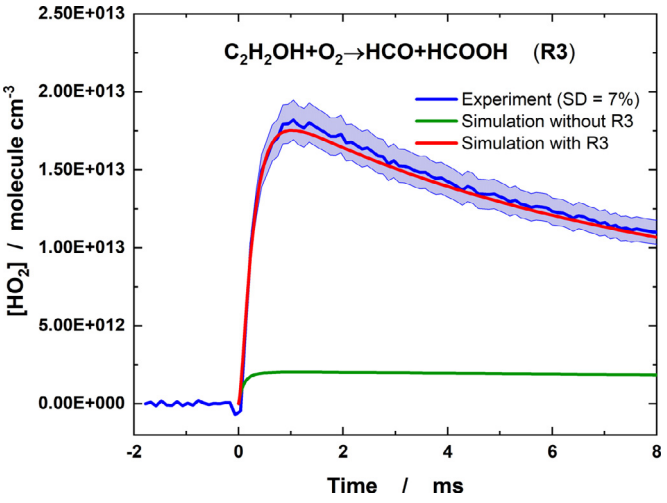

Fig. 6. The temporal profile of HO_2 concentration with a gas mixture of $C_2H_2/O_2/O_3$/He. [C_2H_2] = 2.40 × 10^{16} molecules cm^{-3}. [O_2] = 3.58 × 10^{15} molecules cm^{-3}. [O_3] = 3.28 × 10^{14} molecules cm^{-3}. [$O(^1D)$] = 9.34 × 10^{13} molecules cm^{-3}. A key elementary reaction R3 ($C_2H_2OH + O_2$) dominates the HO_2 formation. The rate constant is determined by comparing the experimental profile with the updated HP-Mech simulation.

The initial concentration of $O(^1D)$ can be quantified based on the photon fluence, the concentration of O_3, and the quantum yield of photodissociation of O_3 at wavelength 266 nm (4th harmonic Nd:Yag laser). The reaction of $O(^1D)$ with C_2H_2 is fast and dominant in the current gas mixture system. The lifetime of this reaction is very short (less than 1 µs). The branching ratios of this reaction are the fitting parameters in this study. The quenching of $CH_2(S)$ by He and C_2H_2 can be finished less than 1 µs time scale. Over 50 transient species in the reaction mechanism are listed in the supporting documents, such as OH, HO_2, CH_2, H, O, HCO, CH_2O, and H_2O. The concentration of stable molecules, O_2, C_2H_2, and O_3 are present in large excess of the transient species (20 ∼ 1000 times). Therefore, the majority initial formed HCCO, $CH_2(S)$, and H in the reaction 1 could convert to OH radicals by the reactions with stable molecule (HCCO+O_2, CH_2+O_2, and $H + O_3$). By comparing the experimental transient profiles of OH radicals with model

Table 1
Branching ratios of reaction 1 at 60 Torr and 296 K. The detailed HP-Mech is listed in the supporting materials. Units are in moles, cubic centimeters, seconds and cal/mole.

Number	Reaction	A	n	Ea	Comments
R1a	$O(^1D) + C_2H_2 \longrightarrow HCCOH$	1.8×10^{14}	0	0	84% of k_{1total}
R1b	$O(^1D) + C_2H_2 \longrightarrow HCCO + H$		0	0	ϕ1b+ϕ1c = (16 ± 4)%
R1c	$O(^1D) + C_2H_2 \longrightarrow CH_2(S) + CO$		0	0	ϕ1b+ϕ1c = (16 ± 4)%
R2	$C_2H_2 + OH + M \longrightarrow C_2H_2OH + M$	2.28×10^{19}	0	1071	Refs. [38,39]
R3a	$C_2H_2OH + O_2 \longrightarrow HCO + HCOOH$	0.74×10^{12}	0	0	Refs. [40]
R3b	$C_2H_2OH + O_2 \longrightarrow HCOHCO + OH$	2.97×10^{12}	0	0	Refs. [40]

simulation using updated HP-Mech, the overall branching ratio of R1b and R1c can be determined.

In Fig. 4, the OH radical absorption was measured at 3568.52 cm^{-1} at 60 Torr and ambient temperature in a $C_2H_2/O_3/O_2$/He gas system. It is interesting to note in Fig. 4 that the peak of OH production is observed 200 μs after photolysis, which indicates that the channel $O(^1D) + C_2H_2 \longrightarrow C_2H + OH$ (R1d) via H abstraction reaction channel forming OH can be neglected because these channels would result in much faster OH rise (ca. 1 μs). This result is different from the previous studies of $O(^1D)$ reaction with saturated hydrocarbons [9,14,37], suggesting the uniqueness of $O(^1D)$ reaction with with alkyne.

According to the simulation based on the reaction mechanism (HP-Mech), the chain branching and propagation channels 1b and 1c, as mentioned in the introduction, have similar sensitivities of OH formation, while the channel 1a is dominant chain termination pathway. As a result, through a adjustment of the ratio of branching ratio ϕ1a/(ϕ1b+ϕ1c), the agreement between simulation and experimental data was greatly improved. However, only an overall chain branching ratios, ϕ1b+ϕ1c, can be determined since both of the channel 1b and 1c result in the fast OH radical formations. The derived branching ratio of channel 1a is 84% and the overall branching ratio of channel 1b and channel 1c is (16 ± 4) % under 60 Torr and ambient temperature conditions. Under higher pressure experiments condition (150 Torr), the measured overall branching ratio of Channel 1b and 1c is (10 ± 3) %. Unimolecular reaction with chemical activation can be analyzed by the ratios of stabilization/dissociation. The collision efficiency and bath gas number density are linearly proportional to the ratio of stabilization/dissociation. Comparing with experiments between 60 Torr and 150 Torr conditions, the decomposition channels are decreased. It should be noted that the HP-Mech was updated in this study, some key elementary reactions were either added or corrected based on most recent literature values (shown in Table 1).

Figure 5 shows the H_2O formation measured using TDLAS at 3568.29 cm^{-1} to validate the updated kinetic mechanism (HP-Mech) which including the branching ratios of $O(^1D)$ reaction with C_2H_2 and key elementary reactions shown in Table 1. The reaction of $CH_2 + O_2 \longrightarrow H_2O + CO$ is the major H_2O formation channel at the initial 150 μs time range and the reaction of $OH + HO_2 \longrightarrow H_2O + O_2$ is the major H_2O formation reaction over 150 μs to 5 ms time range. The simulation agrees well with experimental measurements, especially during the initial H_2O rise but slightly over-predicts the H_2O concentration at around 1 ms. Signal fluctuation is observed from the minor drifting of the laser wavelength which can not be subtracted by the background measurements.

The path flux analysis indicated that the original mechanism constructed using HP-Mech and ozone measurements with additional reactions involving $O(^1D)$ has little sensitivity to the production of HO_2, suggesting the absence of some critical reaction channels for HO_2. A key reaction of C_2H_2OH with O_2 has been added into the reaction mechanism which directly influences the formation of HO_2:

$$C_2H_2OH + O_2 \longrightarrow HCO + HCOOH \quad (10)$$

$$C_2H_2OH + O_2 \longrightarrow HCOHCO + OH \quad (11)$$

In fact, Fig. 6 shows dramatically improved agreement between HO_2 measurements and the model prediction after including reaction $C_2H_2OH + O_2 \longrightarrow HCO + HCOOH$ (R3a) and $C_2H_2OH + O_2 \longrightarrow HCOHCO + OH$ (R3b). The reaction R3 is directly sensitive towards the HCO radical production, which is one of the most important intermediates in HO_2 formation. The experimental errors were mainly introduced from magnetic field (± 10 G) and pathlength (± 21 cm) uncertainty, in total 7%. Sensitivity analysis has been carried out for all reactions in the reaction mechanism. Among the reactions included in the mechanism, some reactions have only marginal importance, while most of them are not important at all. Turning off all other HO_2 formation channels results in the change of the peak value of HO_2 not exceeding 15 %.

The branching ratios and rate constants of key reactions examined in this study are summarized in Table 1.

4. Conclusion

In conclusion, the kinetics of $O(^1D)$ reactions with C_2H_2 are studied through quantitative time-resolved measurements of HO_2, OH, and H_2O in a newly developed photolysis flow reactor. In particular, selective and time-resolved detection of HO_2 was successfully demonstrated through use of Faraday rotation spectroscopy by the suppression of spectral interference from non-paramagnetic hydrocarbon absorption via balanced detection. The branching ratios of $O(^1D)$ reactions with C_2H_2 as well as its subsequent reaction kinetics are quantified.

With the adoption of these reaction channels and the measured reaction rates and branching ratios, an updated kinetic model for $O(^1D)$ reactions with C_2H_2 based on HP-Mech is developed. The updated model significantly improved the prediction of experimental results of OH, HO_2, and H_2O. The results also demonstrate that the new experimental apparatus combing TDLAS with FRS in the photolysis reactor has the potential for sensitive measurements of many species, (e.g. OH, HO_2, H_2O, CH_2O, C_2H_2, and O_3) for the study more complicated chemical kinetics and dynamics involving $O(^1D)$ reaction with large unsaturated hydrocarbons and oxygenated fuels. Furthermore, understanding of $O(^1D)$ reactions with fuels provides a key sub-mechanism of reaction kinetics for combustion, plasma chemistry, materials synthesis, and atmospheric chemistry.

Declaration of Competing Interest

The authors declare that they have no known competing financial interests or personal relationships that could have appeared to influence the work reported in this paper.

Acknowledgment

This project is supported by the NSF grants CBET 1903362 and 1507358, DOE grant DE-SC0020233 of Plasma Science Center, Princeton SEAS innovation grant, ACEE center grant, and Exxon Mobile research grant.

Supplementary material

Supplementary material associated with this article can be found, in the online version, at doi:10.1016/j.combustflame.2019.10.034.

References

[1] E.J. Dunlea, A. Ravishankara, Kinetic studies of the reactions of O(^{1}D) with several atmospheric molecules, Phys. Chem. Chem. Phys. 6 (9) (2004) 2152–2161.
[2] S. Vranckx, J. Peeters, S. Carl, Kinetics of O(^{1}D) + H_2O and O(^{1}D) + H_2: absolute rate coefficients and O(^{3}P) yields between 227 and 453 K, Phys. Chem. Chem. Phys. 12 (32) (2010) 9213–9221.
[3] Y. Ju, W. Sun, Plasma assisted combustion: Dynamics and chemistry, Prog. Energy Combust. Sci. 48 (2015) 21–83.
[4] S. Yang, S. Nagaraja, W. Sun, V. Yang, Multiscale modeling and general theory of non-equilibrium plasma-assisted ignition and combustion, J. Phys. D: Appl. Phys. 50 (43) (2017) 433001.
[5] S. Yang, X. Gao, V. Yang, W. Sun, S. Nagaraja, J.K. Lefkowitz, Y. Ju, Nanosecond pulsed plasma activated C_2H_4/O_2/Ar mixtures in a flow reactor, J. Propuls. Power (2016) 1240–1252.
[6] W. Sun, X. Gao, B. Wu, T. Ombrello, The effect of ozone addition on combustion: Kinetics and dynamics, Prog. Energy Combust. Sci. 73 (2019) 1–25.
[7] M.J. Prather, Time scales in atmospheric chemistry: coupled perturbations to N_2O, NO_y, and O_3, Science 279 (5355) (1998) 1339–1341.
[8] S. Gligorovski, R. Strekowski, S. Barbati, D. Vione, Environmental implications of hydroxyl radicals (OH), Chem. Rev. 115 (24) (2015) 13051–13092.
[9] C. Lin, W. DeMore, Reactions of atomic oxygen (1D) with methane and ethane, J. Phys. Chem. 77 (7) (1973) 863–869.
[10] A. Luntz, Chemical dynamics of the reactions of O(^{1}D2) with saturated hydrocarbons, J. Chem. Phys. 73 (3) (1980) 1143–1152.
[11] H. Yamazaki, R. Cvetanović, Collisional deactivation of the excited singlet oxygen atoms and their insertion into the CH bonds of propane, J. Chem. Phys. 41 (12) (1964) 3703–3710.
[12] X. Yang, Multiple channel dynamics in the O(^{1}D) reaction with alkanes, Phys. Chem. Chem. Phys. 8 (2) (2006) 205–215.
[13] H.-G. Yu, J.T. Muckerman, Mrci calculations of the lowest potential energy surface for CH_3OH and direct ab initio dynamics simulations of the O(^{1}D) + CH_4 reaction, J. Phys. Chem. A 108 (41) (2004) 8615–8623.
[14] S.-i. Wada, K. Obi, Photochemical reaction dynamics of O(^{1}D) with saturated hydrocarbons, CH_4, C_2H_6, and C_3H_8, under bulk conditions and in van der waals complexes, J. Phys. Chem. A 102 (20) (1998) 3481–3491.
[15] S.A. Carl, A highly sensitive method for time-resolved detection of O(^{1}D) applied to precise determination of absolute O(^{1}D) reaction rate constants and O(^{3}P) yields, Phys. Chem. Chem. Phys. 7 (24) (2005) 4051–4053.
[16] Y. Girard, P. Chaquin, Addition reactions of 1D and 3P atomic oxygen with acetylene. potential energy surfaces and stability of the primary products. is oxirene only a triplet molecule? A theoretical study, J. Phys. Chem. A 107 (48) (2003) 10462–10470.
[17] D. Nuñez-Reyes, K.M. Hickson, Rate constants and H-atom product yields for the reactions of O(^{1}D) atoms with ethane and acetylene from 50 to 296 K, J. Phys. Chem. A 122 (20) (2018) 4696–4703, doi:10.1021/acs.jpca.8b02267. PMID: 29715024
[18] M.-W. Chen, B. Rotavera, W. Chao, J. Zádor, C.A. Taatjes, Direct measurement of OH and HO2 formation in R+ O_2 reactions of cyclohexane and tetrahydropyran, Phys. Chem. Chem. Phys. 20 (16) (2018) 10815–10825.
[19] J.D. DeSain, A.D. Ho, C.A. Taatjes, High-resolution diode laser absorption spectroscopy of the O–H stretch overtone band (2, 0, 0)(0, 0, 0) of the HO_2 radical, J. Mol. Spectrosc. 219 (1) (2003) 163–169.
[20] T. Wallington, P. Dagaut, M. Kurylo, Uv absorption cross sections and reaction kinetics and mechanisms for peroxy radicals in the gas phase, Chem. Rev. 92 (4) (1992) 667–710.
[21] D.E. Heard, M.J. Pilling, Measurement of OH and HO_2 in the troposphere, Chem. Rev. 103 (12) (2003) 5163–5198.
[22] K. Clemitshaw, A review of instrumentation and measurement techniques for ground-based and airborne field studies of gas-phase tropospheric chemistry, Crit. Rev. Environ. Sci. Technol. 34 (1) (2004) 1–108.
[23] J. Thiebaud, C. Fittschen, Near infrared cw-CRDS coupled to laser photolysis: spectroscopy and kinetics of the HO_2 radical, Appl. Phys. B 85 (2,3) (2006) 383–389.
[24] J.D. DeSain, S.J. Klippenstein, J.A. Miller, C.A. Taatjes, Measurements, theory, and modeling of OH formation in ethyl+ O_2 and propyl+ O_2 reactions, J. Phys. Chem. A 107 (22) (2003) 4415–4427.
[25] S.A. Nizkorodov, W.W. Harper, B.W. Blackmon, D.J. Nesbitt, Temperature dependent kinetics of the $OH/HO_2/O_3$ chain reaction by time-resolved ir laser absorption spectroscopy, J. Phys. Chem. A 104 (17) (2000) 3964–3973.
[26] C. Yan, S. Kocevska, L.N. Krasnoperov, Kinetics of the reaction of CH_3O_2 radicals with OH studied over the 292–526 K temperature range, J. Phys. Chem. A 120 (31) (2016) 6111–6121.
[27] B. Brumfield, W. Sun, Y. Ju, G. Wysocki, Direct in situ quantification of HO_2 from a flow reactor, J. Phys. Chem. Lett. 4 (6) (2013) 872–876.
[28] B. Brumfield, G. Wysocki, Faraday rotation spectroscopy based on permanent magnets for sensitive detection of oxygen at atmospheric conditions, Opt. Express 20 (28) (2012) 29727–29742.
[29] X. Shen, X. Yang, J.S. Santner, J. Sun, Y. Ju, Experimental and kinetic studies of acetylene flames at elevated pressures, 52nd Aerospace Sciences Meeting (2014), p. 0129.
[30] H. Zhao, X. Yang, Y. Ju, Kinetic studies of ozone assisted low temperature oxidation of dimethyl ether in a flow reactor using molecular-beam mass spectrometry, Combust. Flame 173 (2016) 187–194.
[31] S. Sander, D. Golden, M. Kurylo, G. Moortgat, P. Wine, A. Ravishankara, C. Kolb, M. Molina, B. Finlayson-Pitts, R. Huie, et al., Chemical kinetics and photochemical data for use in atmospheric studies evaluation number 15, Technical Report, Jet Propulsion Laboratory, National Aeronautics and Space Administration, Pasadena, CA, 2006.
[32] J. Westberg, G. Wysocki, Cavity ring-down faraday rotation spectroscopy for oxygen detection, Appl. Phys. B 123 (5) (2017) 168.
[33] A.C. Johansson, J. Westberg, G. Wysocki, A. Foltynowicz, Optical frequency comb faraday rotation spectroscopy, Appl. Phys. B 124 (5) (2018) 79.
[34] C.C. Teng, C. Yan, H. Zhong, A. Rousso, T. Chen, J. Westberg, Y. Ju, G. Wysocki, HO_2 radical measurements in a photolysis reactor using line-locked faraday rotation spectroscopy, Optics and Photonics for Energy and the Environment, Optical Society of America (2018), pp. EW3A–6.
[35] I.E. Gordon, L.S. Rothman, C. Hill, R.V. Kochanov, Y. Tan, P.F. Bernath, M. Birk, V. Boudon, A. Campargue, K. Chance, et al., The HITRAN2016 molecular spectroscopic database, J. Quant. Spectrosc. Radiat. Transf. 203 (2017) 3–69.
[36] R. Kee, F. Rupley, J. Miller, M. Coltrin, J. Grcar, E. Meeks, H. Moffat, A. Lutz, G. Dixon-Lewis, M. Smooke, 2008. Chemkin-Pro.
[37] C.R. Park, J.R. Wiesenfeld, Full characterization of OH product energetics in the reaction of O(^{1}D2) with hydrocarbons, The Journal of chemical physics 95 (11) (1991) 8166–8177.
[38] K.W. McKee, M.A. Blitz, P.A. Cleary, D.R. Glowacki, M.J. Pilling, P.W. Seakins, L. Wang, Experimental and master equation study of the kinetics of OH+ C_2H_2: Temperature dependence of the limiting high pressure and pressure dependent rate coefficients, J. Phys. Chem. A 111 (19) (2007) 4043–4055.
[39] J.P. Senosiain, S.J. Klippenstein, J.A. Miller, The reaction of acetylene with hydroxyl radicals, J. Phys. Chem. A 109 (27) (2005) 6045–6055.
[40] J. Lockhart, M.A. Blitz, D.E. Heard, P.W. Seakins, R.J. Shannon, Mechanism of the reaction of oh with alkynes in the presence of oxygen, J. Phys. Chem. A 117 (26) (2013) 5407–5418.